Pacific Walker Circulation Variability in Coupled and Uncoupled Climate Models

S. Sandeep[1*], Frode Stordal[1], Prashant D. Sardeshmukh[2,3], and Gilbert P. Compo[2,3]

[1] *Section for Meteorology and Oceanography, Department of Geosciences, University of Oslo, PO Box 1022, 0315 Oslo, Norway.*

[2] *Cooperative Institute for Research in Environmental Sciences (CIRES) University of Colorado, Boulder, CO 80309, USA*

[3] *Physical Sciences Division, Earth System Research Laboratory, National Oceanic and Atmospheric Administration, Boulder, CO 80305 USA*

*Present affiliation: *Center for Prototype Climate Modeling, New York University Abu Dhabi, UAE*

Corresponding author email: sandeep.sukumaran@geo.uio.no, sandeep.sukumaran@nyu.edu

Citation:

Sandeep, S., F. Stordal, P. D. Sardeshmukh, and G. P. Compo, 2014: Pacific Walker Circulation variability in coupled and uncoupled climate models. *Climate Dynamics*, doi: 10.1007/s00382-014-2135-3

This article is published by Springer-Verlag. This author-created version is distributed courtesy of Springer-Verlag. The original version of the article can be accessed from www.link.springer.com at http://link.springer.com/article/10.1007/s00382-014-2135-3

Abstract: There is still considerable uncertainty concerning twentieth century trends in the Pacific Walker Circulation (PWC). In this paper, observational datasets, coupled (CMIP5) and uncoupled (AGCM) model simulations, and additional numerical sensitivity experiments are analyzed to investigate twentieth century changes in the PWC and their physical mechanisms. The PWC weakens over the century in the CMIP5 simulations, but strengthens in the AGCM simulations and also in the observational twentieth century reanalysis (20CR) dataset. It is argued that the weakening in the CMIP5 simulations is not a consequence of a reduced global convective mass flux expected from simple considerations of the global hydrological response to global warming, but is rather due to a weakening of the zonal equatorial Pacific sea surface temperature (SST) gradient. Further clarification is provided by additional uncoupled atmospheric general circulation model simulations in which the ENSO-unrelated and ENSO-related portions of the observed SST changes are prescribed as lower boundary conditions. Both sets of SST forcing fields have a global warming trend, and both sets of simulations produce a weakening of the global convective mass flux. However, consistent with the strong role of the zonal SST gradient, the PWC strengthens in the simulations with the ENSO-unrelated SST forcing, which has a strengthening zonal SST gradient, despite the weakening of the global convective mass flux. Overall, our results suggest that the PWC strengthened during 20th century global warming, but also that this strengthening was partly masked by a weakening trend associated with ENSO-related PWC variability.

Keywords: Pacific Walker Circulation; Hydrological Cycle; ENSO

1. Introduction

The Pacific Walker Circulation (PWC), a planetary-scale east-west overturning atmospheric circulation in the equatorial belt with ascent over the western and descent over the eastern Pacific Ocean, is an important component of the global climate system. There is growing interest in how the PWC has been affected by global warming over the past century (Vecchi and Soden 2007; Vecchi et al. 2006; Meng et al. 2012; Tokinaga et al. 2011; Tokinaga et al. 2012). As yet, however, there is no clear consensus on whether it has weakened, strengthened, or remained unchanged. In an early modeling study, Knutson and Manabe (1995) found that the time-mean upward motion weakened in a 4xCO_2 perturbation experiment, despite a 15% increase of precipitation, in the rising branch of the PWC over the Indo-Pacific Warm Pool, and was accompanied by a reduction of the zonal sea surface temperature (SST) gradient along the equatorial Pacific. Held and Soden (2006) argued that a general slowdown of overturning atmospheric circulations was physically necessary to reconcile the much weaker response of global precipitation to global warming compared to the ~ 7% / K increase of saturation water vapor pressure obtained in many climate models. Based on this theoretical expectation, Vecchi and Soden (2007) linked the weakening of the PWC in their climate model simulations (and also apparently in observations) to a global reduction of the convective mass flux. They further noted that the conditions over the tropical Pacific resembled an El Niño-like situation in a warming climate. The fact that they could also simulate a PWC weakening in an atmospheric GCM coupled to a slab ocean instead of a dynamic ocean suggested that it was not strongly influenced by ocean dynamics.

More recent studies have yielded conflicting results regarding twentieth century PWC trends. Some have supported the weakening theory (Tokinaga et al. 2011; 2012), whereas others have found either no trend (Compo et al. 2011) or a strengthening trend (Luo et al. 2012; Meng et al. 2012; Sohn and Park 2010; Wang et al. 2012; L'Heureux et al. 2013). However, because these studies covered different time periods, direct intercomparisons are inappropriate. Given the existence of substantial natural variability on multi-decadal scales in the climate system, it is clearly inappropriate to compare trends obtained over relatively short (30-yr) intervals with those over longer (~100-yr) intervals that are likely more associated with radiatively forced climate change (L'Heureux et al. 2013).

It is important to note in this context that there is also uncertainty in how global warming has affected and will affect tropical Pacific SSTs, with some climate models generating an El Niño-like and others a La Niña-like response (Collins 2005; Latif and Keenlyside 2009; Collins et al. 2010). Multi-model ensemble mean responses often resemble an El Niño-like pattern (Knutson and Manabe 1995; Solomon et al. 2007; Xie et al. 2010). A robust evaluation of the models is complicated by uncertainties in observational SST reconstructions, including disagreements as to whether the eastern equatorial Pacific warmed or cooled over the 20th century (Deser et al. 2010). These disagreements have been shown to be largely associated with differences in the representation of the El Niño Southern Oscillation (ENSO) in the SST reconstructions. When the ENSO-related variations are removed, the residual ENSO-unrelated 20th century SST trend patterns indicate a strengthening of the zonal Pacific SST gradient (Compo and Sardeshmukh 2010; Solomon and Newman 2012), consistent with previous studies that found a strengthening of the full and the ENSO-unrelated zonal SST gradient in some datasets (Cane et al. 1997; Guan and Nigam 2008). Interestingly, the associated ENSO-unrelated trend pattern of Sea Level Pressure (SLP) does not indicate a clear trend in an SLP-based index of the PWC (Solomon and Newman 2012). This suggests that (mis-) representations of ENSO-related variability in observational datasets may have contributed substantially to the disagreements regarding 20th century PWC variability and trends. An investigation of 20th century PWC variability in coupled climate model simulations (Power and Kociuba 2011) found that 30 to 70% of the simulated PWC weakening was accounted for by external forcing and the rest by internal model variability, and that models with relatively weak negative PWC trends were also generally deficient in simulating ENSO.

The disagreements among observational and modeling studies concerning the long-term PWC trend have generated a vigorous debate as to whether the observations or models are in error. Tokinaga et al. (2012) argued that uncoupled AGCMs fail to simulate a weakening of the PWC because of errors in the observational SSTs that are used to force those models. To support their argument, they forced their particular AGCMs with trends in observed night-time marine air temperatures blended with SSTs, and obtained a weakening of the PWC. L'Heureux et al. (2013), on the other hand, questioned the long-term weakening of the PWC itself claimed in observational studies, stressing that biases in the SLP observations and reconstructions compromise those claims, given especially the low signal-to-noise ratios associated with sparse *in situ* measurements before the 1950s. Focusing on the better-observed period since 1950, they found that the PWC has strengthened, not weakened. Observational SLP data quality issues were also raised by DiNezio et al. (2013), who found the PWC weakening trend in the CMIP5 coupled model simulations to be an order of magnitude smaller than in observations and reconstructions. Given that only 26 of the 101 CMIP5 simulations analyzed by them were consistent with the observed PWC trend, they suggested that the weakening trend in the observations could be a result of biases over data sparse oceanic regions such as the region around Tahiti, which is data-poor before the 1940s.

Meng et al. (2012) examined 20th century PWC variability in observations and in a suite of uncoupled atmospheric GCM simulations. They found that the Pacific SST gradient, rather than external radiative forcing *per se*, drove the PWC variability and that the PWC strengthened, not weakened, over the century. However, Tokinaga et al. (2011; 2012), using in situ ocean and land observations concluded that the PWC weakened over the second half of the century. Tokinaga et al. (2011) also found a reduction of land precipitation over the maritime continent, which is inconsistent with the model results of Knutson and Manabe (1995), who obtained an increase in this general area in their 4xCO2 experiment. Knutson and Manabe reconciled their precipitation increase (and the associated increase of latent heat release) with the weakening of upward motion (and associated slowdown of the PWC) by noting an increase also of the static stability and radiative cooling in the region. Their results were thus not inconsistent with the dominant heat balance in areas of organized deep convection in the tropics between diabatic heating and the adiabatic cooling of ascent.

The above very brief summary of the current inadequate understanding of long-term PWC variability and trends is in sharp contrast to the understanding of shorter-term interannual PWC variability. On interannual time scales the PWC, regardless of whether it is defined in terms of vertical velocities in its vertical branches, or zonal winds or pressure gradients in its horizontal branches, weakens (strengthens) during El Niño (La Niña) events, and this is associated with a reduction (intensification) of the zonal SST gradient in the equatorial Pacific. On longer time scales, however, other physics and dynamics come into play as noted above, so it is not obvious to what extent a simple relationship between the PWC and the zonal SST gradient still holds (Karnauskas et al. 2009).

We have three aims in this paper. One is to reassess to what extent the PWC weakened or strengthened over the *entire* 20th century in the longest available observational and reanalysis datasets, and in newly available CMIP5 model simulations (Taylor et al. 2011) performed using the latest generation of coupled models. Our second aim is to determine to what extent the 20th century PWC trends were "ENSO-unrelated" or "ENSO-related", by performing uncoupled atmospheric GCM simulations in which the ENSO-unrelated and

ENSO-related portions of observed global SST anomalies, isolated using the method of Compo and Sardeshmukh (2010) on a month-by-month basis throughout the century, are prescribed as lower boundary conditions. Our third aim is to investigate the tacit assumption made in numerous studies that a weakening of the PWC is necessarily associated with the reduction of the global convective mass flux expected from a weak global mean precipitation response to global warming. In our view, this assumption has been the root cause of skepticism toward observational studies that suggest a long-term strengthening of the PWC, but is in fact unjustified. Our uncoupled atmospheric GCM simulations are especially relevant in this regard. Both our ENSO-unrelated and ENSO-related SST anomaly fields have a global warming trend over the century, and both reduce the global convective mass flux, but the ENSO-unrelated SST forcing strengthens the PWC, whereas the ENSO-related forcing weakens it. This is mainly because over the equatorial Pacific, the ENSO-unrelated trend fields have a steepening zonal SST gradient, whereas the ENSO-related trend fields have a weakening SST gradient.

The data and methods used are summarized in Section 2. This is followed by results and a discussion in Section 3, and concluding remarks in Section 4.

2. Data and methods

We used monthly mean sea level pressure (SLP), convective mass flux (M_c), pressure vertical velocity at 500 hPa (ω_{500}), Surface Temperature (TS), and Sea Surface Temperature (SST) from coupled GCM (CGCM) and uncoupled atmospheric GCM (AGCM) simulations, the Twentieth Century Reanalysis (20CR; (Compo et al. 2011)) dataset, and observational/reconstruction SLP (Allan and Ansell 2006) and SST (Rayner et al. 2003) datasets from the Hadley Center (HadSLP2 and HadISST1.1). We used one ensemble member from each ensemble of simulations generated using 12 different CGCMs (see Table 1) for the CMIP5 project, all spanning the 20th century and using specified observed time-varying concentrations of greenhouse gases (GHGs), ozone, and aerosols as radiative perturbations. We also used four ensemble members of 20th century simulations by an uncoupled AGCM (GISS-E2-R) (Schmidt et al. 2006) participating in the Atmospheric Model Inter-comparison Project (AMIP). The SSTs used in these GISS-E2-R simulations were a merged version of the HadISST1.1 and NOAA OI v2 with HadISST1.1 anomalies plus the NOAA OIv2 (Reynolds et al. 2002) climatology (1971-2000) for data spanning 1871 to November 1981, and the NOAA OIv2 data from December 1981 to the present (Hurrell et al. 2008).

We additionally used a three-member ensemble of AGCM simulations generated in-house with the National Center for Atmospheric Research (NCAR) Community Atmospheric Model version 4 (CAM4), which is the atmospheric component of the Community Earth System Model (CESM1; Gent et al. (2011)). For these simulations, the CAM4 was configured at a horizontal resolution of 0.9^{o} x 1.25^{o} (lat x lon) and 26 hybrid sigma-pressure levels in the vertical. The first ensemble member was generated using observed/reconstructed Hadley Center SSTs and sea ice concentrations (HadISST1.1) as lower boundary conditions, in addition to other 20^{th} century atmospheric forcings used by the coupled models, for the 1900 – 2005 period. The other two ensemble members were generated using Centennial *in situ* Observation-Based Estimates of SST (COBE SST) (Ishii et al. 2005) and NOAA Extended Reconstructed SST version 3 (ERSST v3b) (Smith and Reynolds 2004) SST fields respectively, and with all other forcings identical to those for the first ensemble member. The first year of the model runs was regarded as spin-up and not considered in the subsequent analysis. These CAM4 runs will be referred as control (CTRL) simulations.

In order to estimate the ENSO-related contribution to PWC variability, we performed two sensitivity experiments with the CAM4 model, prescribing time-evolving ENSO-related and ENSO-unrelated monthly SST anomaly fields plus the long-term mean seasonally varying SST fields as lower boundary conditions, and with all other forcings identical to those in the CTRL runs. Each of these experiments consisted of three ensemble members, as in the case of the CTRL experiment. The ENSO-related and ENSO-unrelated SST anomaly fields from HadISST1.1, COBE SST, and ERSST v3b were derived using the dynamical ENSO filter described in Compo and Sardeshmukh (2010).

The PWC index was defined as the difference in area-averaged monthly SLP between the eastern and western Pacific as in Vecchi et al. (2006). The eastern Pacific (160°W – 80°W and 5°S – 5°N) and western Pacific (80°E – 160°E and 5°S – 5°N) areas used for this purpose are shown as rectangular boxes in Fig. 6(a). An index of the zonal equatorial Pacific sea surface temperature gradient (ΔTS) was similarly defined, but using the SST difference between the western and eastern Pacific. The land areas in these regional boxes were masked out in the model and 20CR data when computing ΔTS. The M_c output from the different models was integrated vertically from p_{bottom} = 1000 hPa to p_{top} = 100 hPa and normalized by $P_{bottom} - P_{top}$. The trends in all quantities presented here were calculated using least-squares linear regressions and their level of significance was estimated using a *t*-test. The number of degrees of freedom (*dof*) were adjusted for the lag 1 autocorrelation of the residuals of the linear regression (r_1), when r_1 was significant at the 5% level, as $n' = n(1 - r_1)/(1 + r_1)$, where n' is the adjusted *dof* and n is the original *dof* (Wilks 2011). Unless noted otherwise, all trends and changes stated below as "significant" were estimated to be significant at the 5% level. The multi-model ensemble means of M_c, ω_{500}, and precipitation were computed after regridding to a common 2.5⁰ x 2.5⁰ latitude-longitude grid (using the 'linint2' function in the NCAR Command Language, NCL (NCAR 2012)).

We performed a Clausius-Clapeyron (C-C) scaling of the column integrated water vapor w and precipitation as in Held and Soden (2006). The values of M_c were similarly scaled. The mean responses of w, precipitation, and M_c were determined as differences between 1996–2005 averages and 1901–1910 averages, similar to Held and Soden (2006) and Vecchi and Soden (2007).

For ease of discussion below we quantified the similarities of the SLP, M_c, ω_{500}, and TS trend fields in the uncoupled CAM4 and coupled CMIP5 simulations in terms of the centered spatial correlations (Wilks 2011) of these fields over the oceanic regions of the tropics (30°S – 30°N).

3. Results and discussion

The close relationship between the zonal SST gradient and easterly Trade Winds over the equatorial Pacific, which are an important component of the PWC, is well known (Bjerknes 1966; Lindzen and Nigam 1987). Fig. 1 compares the 20th century variability of ΔTS and the SLP-based PWC index in the statistical reconstructions, 20CR, and model simulations. The curves show anomalies from the long-term mean annual cycle, and the straight lines are least-squares linear trends. Fig. 1a shows a significant ($p < 0.05$) weakening PWC trend (-4 Pa decade^{-1}) in the HadSLP2 dataset and an apparently inconsistent strengthening ΔTS trend (0.04 K decade^{-1}, $p < 0.05$) in the HadSST1.1 dataset. As already discussed in the introduction, errors in the SST, SLP, or both reconstructions could be behind this apparent inconsistency. A possibility of opposite SST and SLP trends involving ocean dynamical mechanisms has also been suggested previously (Karnauskas et al. 2009), but we cannot confirm that the strengthening of ΔTS presented here resulted from an ocean dynamical process. Note also that although the trends in the PWC and ΔTS reconstructions are opposite, the two time series themselves are positively correlated with a correlation coefficient R of 0.66. Strengthening ΔTS trends are seen in other SST reconstructions, such as the ERSST3 (0.01 K decade^{-1}) and COBE SST (0.03 K decade^{-1}) datasets as well, although only the latter is statistically significant at the 5% level. The PWC and ΔTS time series derived from the 20CR, shown in Fig. 1b, both show significant strengthening trends, and the time series are well correlated (R = 0.84). It should be noted that the 20CR uses HadISST1.1 as the SST boundary condition in its data assimilation system (Compo et al. 2011). The ensemble means of the three CAM4 CTRL simulations shown in Fig. 1c also have significant strengthening trends in the PWC and ΔTS, and the two time series are highly correlated (R = 0.93). Note that the strengthening ΔTS trend in Fig. 1c reflects an average over three different observational SST datasets: HadISST1.1, COBE, and ERSSTv3b. The strengthening of the PWC in the 20CR and CTRL simulations is consistent with the results of Meng et al. (2012). On the other hand, the CMIP5 model simulations (Fig. 1d) show slight but statistically significant weakening trends in both the PWC and ΔTS. Similar to Figs 1b and 1c, the ensemble-mean CMIP5 PWC and ΔTS time series in Fig. 1d are also highly correlated (R=0.89). Indeed this is also true for the individual models in the CMIP5 ensemble, with R ranging between 0.7 (GFDL-ESM2G) and 0.93 (CCSM4). The weakening ensemble-mean PWC trend in this CMIP5 ensemble is consistent with previously reported weakening trends in coupled model simulations with anthropogenic forcing (Vecchi et al. 2006); however, its magnitude is smaller (~ -1.7 Pa decade^{-1} vs. ~ -2.5 Pa decade^{-1}, see Fig. 2 in Vecchi et al. (2006)).

We next estimate the ENSO-related PWC variability by considering the CAM4 model forced with ENSO-related and ENSO-unrelated SSTs in two separate sensitivity experiments. The ENSO-related SST anomalies were filtered on a month-by-month basis from the HadISST1.1, COBE SST, and ERSST v3b data using a novel method, which unlike conventional regression or band-pass filtering methods does not define ENSO in terms of a single index or temporal frequency, but rather treats it as an evolving dynamical process (Penland and Matrosova (2006); Penland and Sardeshmukh (1995); see Compo and Sardeshmukh (2010) for details). Fig. 2a shows that both the PWC and ΔTS have significant weakening trends in the ensemble mean of the three CAM4 simulations forced with the ENSO-related SSTs. On the other hand, as shown in Fig. 2b, they both have strengthening trends in the simulations forced with the ENSO-unrelated SSTs that are consistent with the strengthening trends in the 20CR dataset and CTRL simulations in Fig. 1. The PWC has an ensemble mean trend of about 2.3 Pa/decade in the CTRL ensemble, and about 10.1 and -7.4 Pa/decade in the ENSO-unrelated and ENSO-related SST forced ensembles, respectively. Note that the strengthening ENSO-unrelated ΔTS trend in Fig. 2b is the dominant contributor to the strengthening full ΔTS trend in Fig. 1a-c.

These intercomparisons of long-term trends in Figs. 1 and 2 suggest a dominant role of ENSO-unrelated SST changes in the dynamics of the PWC trend. They also suggest that the large ENSO-related PWC variability compromises the estimation of the PWC trend, depending on how that variability is represented in observational datasets of limited length and quality. This is evident from the similar large magnitudes of interannual PWC variability in the reconstruction and 20CR datasets and CTRL simulations in Fig. 1 and the ENSO-related PWC variability in Fig. 2a.

As already mentioned, a weakening of the PWC has generally been assumed to be associated with a global slowdown of overturning atmospheric circulations, i.e., a decrease of global mean M_c, expected from the relatively muted response of global mean precipitation (compared to that of global mean column integrated water vapor) to global warming. Here we investigate how closely the PWC changes follow those of the globally, as well as tropically, averaged M_c in the model simulations. In the CTRL simulations (Fig. 3a), both the globally and tropically averaged M_c show significant decreasing trends, that are relatively large over the second half of the century. The simulated PWC time series is repeated in Fig. 3a for convenience, and all time series are presented as 36 month running means for clarity. The correlation between the PWC and globally (tropically) averaged M_c time series is -0.03 (0.24), which indicates a very weak association between the two variables. The same analysis repeated for a four-member ensemble mean of uncoupled GISS-E2-R AMIP (Schmidt et al. 2006) simulations (Fig. 3b) yields similar results, with a statistically significant weakening of tropically and globally averaged M_c and strengthening of the PWC. As in the case of the CTRL simulations using CAM4, the PWC in the GISS-E2-R ensemble is also poorly correlated with the global M_c (R = 0.07) as well as the tropical M_c (R = 0.26). The CMIP5 ensemble (Fig. 3c) shows a weakening of both the globally and tropically averaged M_c, in agreement with previous model studies (Held and Soden 2006; Vecchi and Soden 2007). However, the relationship between the PWC and M_c is weak, considering the much smaller magnitude of the PWC trend here than in the CTRL runs and also the weak correlation of the two time series, with R = 0.15 (0.28) for the globally (tropically) averaged M_c. The PWC and M_c in the CMIP5 simulations are somewhat better correlated at longer time scales (10-yr running means) with R = 0.44 (0.44) for global (tropical) averages. However, the corresponding correlations of R = -0.16 (-0.04) remain weak in the CTRL simulations.

The M_c and PWC changes in the ENSO-related and ENSO-unrelated SST forcing experiments are shown in Fig. 4. The globally and tropically averaged M_c weaken significantly over the century in both experiments. However, the PWC weakens in the ENSO-related forcing experiment (Fig. 4a) whereas it strengthens in the ENSO-unrelated forcing experiment (Fig. 4b). The correlations of the PWC and globally (tropically) averaged M_c time series are 0.13 (0.42) in the ENSO-related forcing experiment and -0.25 (-0.1) in the ENSO-unrelated forcing experiment.

Taken together, the results in Figures 3 and 4 suggest a rather tenuous relationship between the PWC and the globally or tropically averaged convective mass flux M_c. They highlight the danger of linking global energy balance constraints to regional phenomena such as the Pacific Walker Circulation. Tokinaga et al. (2012) also suggested that the PWC trend is more closely associated with the trend in the Indo-Pacific SST gradient, rather than the reduction in global mean M_c.

To assess the consistency of the simulated changes in M_c with the scaling arguments of Held and Soden (2006), we related the global mean responses of precipitation, column integrated water vapor, and M_c to the change in global mean TS in each of our datasets (Table 2). The difference (1996–2005 average minus

1901–1910 average) in global mean TS (δTS) yields a value of 0.90 K for the coupled CMIP5 ensemble, which is closely matched by the δTS of 0.91K for the uncoupled CTRL ensemble. The ENSO-related and ENSO-unrelated ensembles show a weaker warming with δTS values of 0.52 K and 0.64 K respectively. The scaled responses of the global mean precipitation to δTS are 1.2 % K^{-1}, 1.6 % K^{-1}, 0.4 % K^{-1}, and 0.2 % K^{-1} respectively in the CMIP5, CTRL, ENSO-related, and ENSO-unrelated simulations. The responses in the CMIP5 and CTRL simulations are consistent with the precipitation responses in the 1 – 2 % K^{-1} range reported by Held and Soden (2006) for the A1B scenario simulations of the CMIP3 coupled models. The weaker responses in the ENSO-related and ENSO-unrelated simulations are not surprising, since they each specify only a part of the δTS changes, and only over the oceans. Nonetheless, the substantial response to the ENSO-related SST changes suggests that ENSO plays an important role in the variability of even global mean precipitation.

The scaled responses of column-integrated water vapor range between 7 % K^{-1} and 7.4 % K^{-1} in the CMIP5, CTRL, and ENSO-related simulations, consistent with previous studies (e.g. (Held and Soden 2006; Vecchi and Soden 2007), although the 5.5 % K^{-1} response obtained in the ENSO-unrelated simulations is somewhat weaker. The scaled M_c responses of -3.1 % K^{-1} (CMIP5), -2.4 % K^{-1} (CTRL), -4.7 % K^{-1} (ENSO-related), and -2.4 % K^{-1} (ENSO-unrelated) show a reduction of M_c in not just the coupled but in all the uncoupled simulations as well. Consistent with the arguments for a reduction in global M_c, the (ENSO-related forcing) experiment with the largest difference between the scaled responses of global mean column integrated water vapor and precipitation also has the largest scaled reduction in M_c, and experiments with relatively weaker differences between δw/δTS and δP/δTS have relatively weaker scaled reductions in M_c.

The time series of δTS and the fractional changes of global precipitation (δP/P), column integrated water vapor (δw/w), and convective mass flux ($\delta M_c/M_c$) are shown in Fig. 5 for the four sets of simulations. The increases of δw/w (Fig. 5c) with increases of δTS (Fig. 5a) in all simulations are generally consistent with C-C scaling. The decreases of $\delta M_c/M_c$ (Fig. 5d) in all simulations are also consistent with the weak increases of δP/P (Fig. 5b) according to the global energy balance arguments of Held and Soden (2006).

It is interesting to examine the spatial patterns of the SLP, TS, and M_c trends, and also of the ω_{500} and precipitation trends, to better understand the above results in a larger geographical context. The 1901–2005 linear trends of these quantities in the CTRL simulations are shown in Fig. 6. Focusing on the 10^oS-10^oN equatorial zone, it is clear that the strong positive SLP trend over the eastern Pacific and the weak positive and negative trends over the maritime continent are both responsible for the strengthening of the PWC in the CTRL simulations. The trend patterns of vertical velocity (Fig. 6b) and convective mass flux (Fig. 6c) are consistent with that of SLP (Table 3). Further, the surface warming trend over the western Pacific, and the slight cooling trend over the eastern Pacific (Fig. 6d), both contribute to steepening the zonal SST gradient over the equatorial Pacific. Together, these results indicate a robust strengthening PWC trend associated with both enhanced ascent in its ascending branch and enhanced descent in its descending branch, and with enhanced zonal SLP and SST gradients in its surface branch. Considering the wider tropical belt (30^oS-30^oN), it is evident that the convective mass flux M_c has a larger area of negative trends than positive trends, which contributes to a general weakening of M_c as highlighted in Fig. 5d. Figures 5d and 6 show that a general weakening of area averaged M_c can be compatible with a strengthening of the PWC. This suggests that air-sea interactions over the tropical Pacific dominated over radiative forcing in determining the PWC variability and trend over the 20th century, in line with Xie et al. (2010).

Figure 7 shows the spatial patterns of the trends in the coupled CMIP5 simulations, in an identical format to that of Fig 6. Focusing again on the 10^oS-10^oN equatorial zone, it is evident that the SLP, vertical velocity, convective mass flux, and TS trends have spatial variations that are very different, and generally *opposite*, to those in the CTRL simulations over the Pacific sector. It is particularly interesting that the stronger surface warming trend over the cold tongue region of the eastern equatorial Pacific (Fig. 6d), together with a slightly weaker warming over the western Pacific, resembles an El Niño-like pattern, which was also seen in many of the coupled CMIP3 simulations (Collins 2005; Solomon et al. 2007) as well as in the 4xCO2 experiments of Knutson and Manabe (1995). Together, they indicate a robust *weakening* PWC trend associated with both reduced ascent in its ascending branch and reduced descent in its descending branch, and reduced zonal SLP/SST gradients in its surface branch.

Considering the wider tropical belt (30^{o}S-30^{o}N), the convective mass flux M_c has a larger area of negative trends than positive trends, similar to the CTRL runs but over an even larger area, which makes a major contribution to the general weakening trend of globally and tropically averaged M_c in these CMIP5 simulations.

Table 3 shows the spatial correlations of various pairs of trend patterns in Figs. 6 and 7, computed over the oceanic regions of the tropics (30°S – 30°N). The SLP trend is moderately correlated with the ω_{500} and M_c trends in the CTRL ensemble (R = 0.41 and -0.38) as well as in the CMIP5 ensemble (R = 0.46 and -0.34). The SLP trend is well correlated with the TS trend in the CTRL ensemble (R=-0.73), but moderately correlated in the CMIP5 ensemble (R=-0.4). The ω_{500} and M_c trends are highly correlated in the CTRL ensemble (R=-0.91) and also in the CMIP5 ensemble (R=-0.85). The ω_{500} and TS trends are moderately correlated in the CTRL ensemble (R=-0.46) and also in the CMIP5 ensemble (R=-0.34). Similarly, the M_c and TS trends are moderately correlated in the CTRL ensemble (R=0.49) and in the CMIP5 ensemble (R=0.52). Finally, the trend patterns of SLP in the CTRL and CMIP5 ensembles are less strongly correlated with one another (R=0.36), and those of ω_{500}, M_c, and TS are poorly correlated (R=-0.01, 0.07, and 0.03 respectively).

The spatial correlations presented in Table 3 support the interpretation of the trend patterns in Figs. 6 and 7 that changes of the PWC (defined by an SLP index) cannot be explained by changes of either the globally or tropically averaged convective mass flux. In general, the SLP variability is strongly tied to the TS variability in the uncoupled AGCM simulations, but much less strongly in the coupled CMIP5 simulations. The M_c and ω_{500} variations, on the other hand, are strongly correlated in both AGCM and CMIP5 simulations.

We also computed the linear trends of SLP and ω_{500} in the 20CR dataset. Their patterns are shown in Fig. 8. The SLP trends (Fig. 8a) are broadly consistent with those in the CTRL simulations (Fig. 6a), although they have somewhat larger magnitudes, and also have different signs over Asia. Importantly for our purposes, however, both the 20CR and CTRL SLP trends are positive over the eastern tropical Pacific and negative over the equatorial western Pacific and Indian Oceans. In other words, both SLP trend fields indicate a strengthening PWC trend. The ω_{500} trend pattern in the 20CR dataset (Fig. 8b) is also consistent with that of SLP in terms of strengthening ascent over the maritime continent, in the area of maximum equatorial SLP decrease, and descent over the equatorial eastern Pacific, in the area of maximum equatorial SLP increase. Both of these features are consistent with a strengthening of the PWC.

As a final check that we really do obtain consistently different PWC trend responses in the CTRL simulations with prescribed observed SSTs (with due acknowledgement of their uncertainties) and in the CMIP5 simulations with imposed radiative perturbations in which the SSTs are obtained as part of the response (and which may also have errors), we examine the precipitation trends in the simulations. As noted earlier, Knutson and Manabe (1995) obtained a 15% increase of precipitation over the maritime continent in response to a 4xCO2 forcing. Some observational studies, however, suggest a decreasing recent precipitation trend over the maritime continent (Tokinaga et al. 2011). Our CTRL simulations do not show a significant precipitation trend over the maritime continent (Fig. 9a), but they do show a decreasing precipitation trend over the eastern equatorial Pacific consistent with a strengthening of the PWC. The result for the CMIP5 simulations (Fig. 9b) is a decreasing precipitation trend over the maritime continent and an increasing trend over the central and eastern equatorial Pacific, consistent with a weakening of the PWC. This pattern bears some resemblance to that associated with El Niño events (Dai and Wigley 2000). It is also consistent with the El Niño-like SST warming trend pattern in the CMIP5 simulations (Fig. 6d). The precipitation trend pattern in the uncoupled simulations with ENSO-related SST forcing (Fig. 9c) further supports the notion that the precipitation trend in the CMIP5 simulations is “El Niño-like”, although of much weaker magnitude. The precipitation trend pattern in the uncoupled simulations with ENSO-unrelated SST forcing (Fig. 9d) shows an increasing trend over the western Pacific and a decreasing trend over the central and eastern tropical Pacific, consistent with the strengthening of the PWC.

Similar to our interpretation of the PWC trend, the precipitation trend patterns in Fig. 9 also suggest that the underlying tropical SST trend *pattern*, as opposed to the overall tropical SST warming trend associated with global warming, plays an important role in determining atmospheric circulation trends over the tropical Indo-Pacific. The main reason the PWC trends are opposite in the uncoupled CTRL and coupled CMIP5 simulations is because the trends in the zonal SST gradients are opposite in these simulations, and not because the trends in the global convective mass flux are opposite (they are, in fact, the same).

4. Concluding remarks

In this paper we investigated changes in the Pacific Walker Circulation over the 20th century using observational and reanalysis datasets and coupled (atmosphere-ocean) as well as uncoupled (atmosphere only, prescribed SST) model simulations. Consistent with Meng et al. (2012), our results suggest that changes in the zonal SST gradient over the tropical Pacific, associated with coupled air-sea processes rather than radiative forcing *per se*, are crucial in determining PWC variability and trends. We challenge the notion that a weakening or strengthening PWC trend is strongly tied to a weakening or strengthening of the global convective mass flux M_c. This challenge is justified by the poor correlation of the PWC and M_c variations in the simulations examined here and also the fact that one can obtain a PWC trend of either sign in the presence of a weakening M_c trend. With regard to the question of whether the PWC strengthened or weakened over the 20th century in association with global warming, our results suggest that it strengthened, but that this strengthening was partly masked by a weakening trend associated with ENSO-related PWC variability. We noted that this component of the PWC variability also compromises attempts to pin down the sign of the PWC trend using observational datasets of limited length and quality. The reanalysis data could also be affected by the quality of the observations that are assimilated. We suspect that the weakening PWC trend obtained in the CMIP5 models is ultimately due to their misrepresentation and systematic underestimation of the spatial variation of tropical SST trends (clearly demonstrated by Shin and Sardeshmukh (2011) for the CMIP3 models), but more work is needed to confirm or reject this suspicion.

Acknowledgments: S.S. and F.S. acknowledge the financial support of the Research Council of Norway through the funding of the project SoCOCA (190159/V10). The Norwegian national supercomputing (NOTUR) resources of Hexagon (project nn2345k) and Norstore (project ns2806k) were extensively used in this work. The Twentieth Century Reanalysis Project used resources of the National Energy Research Scientific Computing Center managed by Lawrence

Berkeley National Laboratory and of the Oak Ridge Leadership Computing Facility at Oak Ridge National Laboratory, which are supported by the Office of Science of the U.S. Department of Energy under Contract No. DE-AC02-05CH11231 and Contract No. DE-AC05-00OR22725, respectively. Support for the Twentieth Century Reanalysis Project dataset is provided by the U.S. Department of Energy, Office of Science Innovative and Novel Computational Impact on Theory and Experiment (DOE INCITE) program, and Office of Science (BER), and by the National Oceanic and Atmospheric Administration Climate Program Office. The research of P.D.S. and G.P.C was supported by the Office of Science (BER), U.S. Department of Energy and by the NOAA Climate Program Office. The CMIP5 coupled model simulations were obtained from Program for Climate Modeling Inter-comparison (PCMDI), which is a part of World Climate Research Program, and we thank each modeling group for providing their data. The authors thank J. Hurrell of NCAR for help in understanding differences in SST datasets. For providing their SST data, we thank the Hadley Centre, N. Rayner, and BADC for HadISST, NOAA/NCDC and T. Smith for ERSST, and the JMA and M. Ishii for COBE.

References

Allan R, Ansell T (2006) A New Globally Complete Monthly Historical Gridded Mean Sea Level Pressure Dataset (HadSLP2): 1850–2004. Journal of Climate 19 (22):5816-5842. doi:10.1175/jcli3937.1

Bentsen M, Bethke I, Debernard JB, Iversen T, Kirkevåg A, Seland Ø, Drange H, Roelandt C, Seierstad IA, Hoose C, Kristjánsson JE (2012) The Norwegian Earth System Model, NorESM1-M – Part 1: Description and basic evaluation. Geoscientific Model Development Discussions 5 (3):2843-2931. doi:10.5194/gmdd-5-2843-2012

Bjerknes J (1966) A possible response of the atmospheric Hadley circulation to equatorial anomalies of ocean temperature. Tellus 18 (4):820-829. doi:10.1111/j.2153-3490.1966.tb00303.x

Cane MA, Clement AC, Kaplan A, Kushnir Y, Pozdnyakov D, Seager R, Zebiak SE, Murtugudde R (1997) Twentieth-century sea surface temperature trends. Science 275 (5302):957-960

Chylek P, Li J, Dubey MK, Wang M, Lesins G (2011) Observed and model simulated 20th century Arctic temperature variability: Canadian Earth System Model CanESM2. Atmospheric Chemistry and Physics Discussions 11 (8):22893-22907. doi:10.5194/acpd-11-22893-2011

Collins M (2005) El Niño-or La Niña-like climate change? Climate Dynamics 24 (1):89-104

Collins M, An S-I, Cai W, Ganachaud A, Guilyardi E, Jin F-F, Jochum M, Lengaigne M, Power S, Timmermann A, Vecchi G, Wittenberg A (2010)

The impact of global warming on the tropical Pacific Ocean and El Nino. Nature Geosci 3 (6):391-397

Compo GP, Sardeshmukh PD (2010) Removing ENSO-Related Variations from the Climate Record. Journal of Climate 23 (8):1957-1978. doi:10.1175/2009jcli2735.1

Compo GP, Whitaker JS, Sardeshmukh PD, Matsui N, Allan RJ, Yin X, Gleason BE, Vose RS, Rutledge G, Bessemoulin P, Brönnimann S, Brunet M, Crouthamel RI, Grant AN, Groisman PY, Jones PD, Kruk MC, Kruger AC, Marshall GJ, Maugeri M, Mok HY, Nordli Ø, Ross TF, Trigo RM, Wang XL, Woodruff SD, Worley SJ (2011) The Twentieth Century Reanalysis Project. Quarterly Journal of the Royal Meteorological Society 137 (654):1-28. doi:10.1002/qj.776

Dai A, Wigley TML (2000) Global patterns of ENSO-induced precipitation. Geophysical Research Letters 27 (9):1283. doi:10.1029/1999gl011140

Deser C, Phillips AS, Alexander MA (2010) Twentieth century tropical sea surface temperature trends revisited. Geophysical Research Letters 37 (10). doi:10.1029/2010gl043321

DiNezio PN, Vecchi GA, Clement AC (2013) Detectability of Changes in the Walker Circulation in Response to Global Warming. Journal of Climate:130114154537002. doi:10.1175/jcli-d-12-00531.1

Dunne JP, John JG, Adcroft AJ, Griffies SM, Hallberg RW, Shevliakova E, Stouffer RJ, Cooke W, Dunne KA, Harrison MJ, Krasting JP, Malyshev SL, Milly PCD, Phillipps PJ, Sentman LT, Samuels BL, Spelman MJ, Winton M, Wittenberg AT, Zadeh N (2012) GFDL's ESM2 Global Coupled Climate–Carbon Earth System Models. Part I: Physical Formulation and Baseline Simulation Characteristics. Journal of Climate 25 (19):6646-6665. doi:10.1175/JCLI-D-11-00560.1

Gent PR, Danabasoglu G, Donner LJ, Holland MM, Hunke EC, Jayne SR, Lawrence DM, Neale RB, Rasch PJ, Vertenstein M, Worley PH, Yang Z-L, Zhang M (2011) The Community Climate System Model Version 4. Journal of Climate 24 (19):4973-4991. doi:10.1175/2011jcli4083.1

Griffies SM, Winton M, Donner LJ, Horowitz LW, Downes SM, Farneti R, Gnanadesikan A, Hurlin WJ, Lee H-C, Liang Z, Palter JB, Samuels BL, Wittenberg AT, Wyman BL, Yin J, Zadeh N (2011) The GFDL CM3 Coupled Climate Model: Characteristics of the Ocean and Sea Ice Simulations. Journal of Climate 24 (13):3520-3544. doi:10.1175/2011JCLI3964.1

Guan B, Nigam S (2008) Pacific Sea Surface Temperatures in the Twentieth Century: An Evolution-Centric Analysis of Variability and Trend. Journal of Climate 21 (12):2790-2809. doi:10.1175/2007JCLI2076.1

Held IM, Soden BJ (2006) Robust Responses of the Hydrological Cycle to Global Warming. Journal of Climate 19 (21):5686-5699. doi:10.1175/jcli3990.1

Hurrell JW, Hack JJ, Shea D, Caron JM, Rosinski J (2008) A New Sea Surface Temperature and Sea Ice Boundary Dataset for the Community Atmosphere Model. Journal of Climate 21 (19):5145-5153. doi:10.1175/2008jcli2292.1

Ishii M, Shouji A, Sugimoto S, Matsumoto T (2005) Objective analyses of sea-surface temperature and marine meteorological variables for the 20th century using ICOADS and the Kobe Collection. International Journal of Climatology 25 (7):865-879. doi:10.1002/joc.1169

Karnauskas KB, Seager R, Kaplan A, Kushnir Y, Cane MA (2009) Observed Strengthening of the Zonal Sea Surface Temperature Gradient across the Equatorial Pacific Ocean*. J Climate 22 (16):4316-4321. doi:10.1175/2009jcli2936.1

Knutson TR, Manabe S (1995) Time-mean response over the tropical Pacific to increased C02 in a coupled ocean-atmosphere model. Journal of Climate 8 (9):2181-2199

L'Heureux ML, Lee S, Lyon B (2013) Recent multidecadal strengthening of the Walker circulation across the tropical Pacific. Nature Clim Change 3 (6):571-576. doi:10.1038/nclimate1840

Latif M, Keenlyside NS (2009) El Niño/Southern Oscillation response to global warming. Proceedings of the National Academy of Sciences 106 (49):20578-20583. doi:10.1073/pnas.0710860105

Lindzen RS, Nigam S (1987) On the Role of Sea Surface Temperature Gradients in Forcing Low-Level Winds and Convergence in the Tropics. Journal of the Atmospheric Sciences 44 (17):2418-2436. doi:10.1175/1520-0469(1987)044<2418:otross>2.0.co;2

Luo J-J, Sasaki W, Masumoto Y (2012) Indian Ocean warming modulates Pacific climate change. Proceedings of the National Academy of Sciences 109 (46):18701-18706. doi:10.1073/pnas.1210239109

Meng Q, Latif M, Park W, Keenlyside NS, Semenov VA, Martin T (2012) Twentieth century Walker Circulation change: data analysis and model experiments. Climate Dynamics 38 (9-10):1757-1773. doi:10.1007/s00382-011-1047-8

NCAR (2012) The NCAR Command Language [Software]. 6.0.0 edn. UCAR/NCAR/CISL/VETS, Boulder, CO. doi:10.5065/d6wd3xh5

Penland C, Matrosova L (2006) Studies of El Niño and Interdecadal Variability in Tropical Sea Surface Temperatures Using a Nonnormal Filter. Journal of Climate 19 (22):5796-5815. doi:10.1175/JCLI3951.1

Penland C, Sardeshmukh PD (1995) The Optimal Growth of Tropical Sea Surface Temperature Anomalies. Journal of Climate 8 (8):1999-2024. doi:10.1175/1520-0442(1995)008<1999:TOGOTS>2.0.CO;2

Power SB, Kociuba G (2011) What Caused the Observed Twentieth-Century Weakening of the Walker Circulation? Journal of Climate 24 (24):6501-6514. doi:10.1175/2011jcli4101.1

Rayner NA, Parker DE, Horton EB, Folland CK, Alexander LV, Rowell DP, Kent EC, Kaplan A (2003) Global analyses of sea surface temperature, sea ice, and night marine air temperature since the late nineteenth century. J Geophys Res 108 (D14):4407. doi:10.1029/2002jd002670

Reynolds RW, Rayner NA, Smith TM, Stokes DC, Wang W (2002) An Improved In Situ and Satellite SST Analysis for Climate. Journal of Climate 15 (13):1609-1625. doi:10.1175/1520-0442(2002)015<1609:AIISAS>2.0.CO;2

Richter JH, Sassi F, Garcia RR, Matthes K, Fischer CA (2008) Dynamics of the middle atmosphere as simulated by the Whole Atmosphere Community Climate Model, version 3 (WACCM3). J Geophys Res 113 (D8):D08101. doi:10.1029/2007JD009269

Riley WJ, Subin ZM, Lawrence DM, Swenson SC, Torn MS, Meng L, Mahowald NM, Hess P (2011) Barriers to predicting changes in global terrestrial methane fluxes: analyses using CLM4Me, a methane biogeochemistry model integrated in CESM. Biogeosciences 8 (7):1925-1953. doi:10.5194/bg-8-1925-2011

Schmidt GA, Ruedy R, Hansen JE, Aleinov I, Bell N, Bauer M, Bauer S, Cairns B, Canuto V, Cheng Y, Del Genio A, Faluvegi G, Friend AD, Hall TM, Hu Y, Kelley M, Kiang NY, Koch D, Lacis AA, Lerner J, Lo KK, Miller RL, Nazarenko L, Oinas V, Perlwitz J, Perlwitz J, Rind D, Romanou A, Russell GL, Sato M, Shindell DT, Stone PH, Sun S, Tausnev N, Thresher D, Yao M-S (2006) Present-Day Atmospheric Simulations Using GISS ModelE: Comparison to In Situ, Satellite, and Reanalysis Data. Journal of Climate 19 (2):153-192. doi:10.1175/jcli3612.1

Shin S-I, Sardeshmukh P (2011) Critical influence of the pattern of Tropical Ocean warming on remote climate trends. Climate Dynamics 36 (7-8):1577-1591. doi:10.1007/s00382-009-0732-3

Smith TM, Reynolds RW (2004) Improved Extended Reconstruction of SST (1854–1997). Journal of Climate 17 (12):2466-2477. doi:10.1175/1520-0442(2004)017<2466:IEROS>2.0.CO;2

Sohn BJ, Park S-C (2010) Strengthened tropical circulations in past three decades inferred from water vapor transport. Journal of Geophysical Research 115 (D15). doi:10.1029/2009jd013713

Solomon A, Newman M (2012) Reconciling disparate twentieth-century Indo-Pacific ocean temperature trends in the instrumental record. Nature Clim Change 2 (9):691-699. doi:10.1038/nclimate1591

Solomon S, Qin D, Manning M, Alley RB, Berntsen T, Bindoff NL, Chen Z, Chidthaisong A, Gregory JM, Hegerl GC, Heimann M, Hewitson B, Hoskins BJ, Joos F, Jouzel J, Kattsov V, Lohmann U, Matsuno T, Molina M, Nicholls N, J.Overpeck, Raga G, Ramaswamy V, Ren J, Rusticucci M, Somerville R, Stocker TF, Whetton P, Wood RA, Wratt D (2007) Technical Summary. Climate Change 2007: The Physical Science Basis. Contribution of Working Group I to the Fourth

Assessment Report of the Intergovernmental Panel on Climate Change. IPCC, Cambridge, United Kingdom and New York, NY,USA.

Taylor KE, Stouffer RJ, Meehl GA (2011) An Overview of CMIP5 and the Experiment Design. Bulletin of the American Meteorological Society 93 (4):485-498. doi:10.1175/BAMS-D-11-00094.1

Tjiputra JF, Roelandt C, Bentsen M, Lawrence DM, Lorentzen T, Schwinger J, Seland Ø, Heinze C (2012) Evaluation of the carbon cycle components in the Norwegian Earth System Model (NorESM). Geoscientific Model Development Discussions 5 (4):3035-3087. doi:10.5194/gmdd-5-3035-2012

Tokinaga H, Xie S-P, Deser C, Kosaka Y, Okumura YM (2012) Slowdown of the Walker circulation driven by tropical Indo-Pacific warming. Nature 491 (7424):439-443. doi:10.1038/nature11576

Tokinaga H, Xie S-P, Timmermann A, McGregor S, Ogata T, Kubota H, Okumura YM (2011) Regional Patterns of Tropical Indo-Pacific Climate Change: Evidence of the Walker Circulation Weakening. Journal of Climate 25 (5):1689-1710. doi:10.1175/jcli-d-11-00263.1

Vecchi GA, Soden BJ (2007) Global Warming and the Weakening of the Tropical Circulation. Journal of Climate 20 (17):4316-4340. doi:10.1175/jcli4258.1

Vecchi GA, Soden BJ, Wittenberg AT, Held IM, Leetmaa A, Harrison MJ (2006) Weakening of tropical Pacific atmospheric circulation due to anthropogenic forcing. Nature 441 (7089):73-76. doi:10.1038/nature04744

Wang B, Liu J, Kim H-J, Webster P, Yim S-Y (2012) Recent change of the global monsoon precipitation (1979–2008). Climate Dynamics 39 (5):1123-1135. doi:10.1007/s00382-011-1266-z

Watanabe M, Suzuki T, O'ishi R, Komuro Y, Watanabe S, Emori S, Takemura T, Chikira M, Ogura T, Sekiguchi M, Takata K, Yamazaki D, Yokohata T, Nozawa T, Hasumi H, Tatebe H, Kimoto M (2010) Improved Climate Simulation by MIROC5: Mean States, Variability, and Climate Sensitivity. Journal of Climate 23 (23):6312-6335. doi:10.1175/2010jcli3679.1

Wilks DS (2011) Statistical methods in the atmospheric sciences, vol 100. Academic press, Waltham, MA

Wu T (2012) A mass-flux cumulus parameterization scheme for large-scale models: description and test with observations. Climate Dynamics 38 (3-4):725-744. doi:10.1007/s00382-011-0995-3

Xie S-P, Deser C, Vecchi GA, Ma J, Teng H, Wittenberg AT (2010) Global Warming Pattern Formation: Sea Surface Temperature and Rainfall. Journal of Climate 23 (4):966-986. doi:10.1175/2009JCLI3329.1

Yukimoto S, Adachi Y, Hosaka M, Sakami T, Yoshimura H, Hirabara M, Tanaka TY, Shindo E, Tsujino H, Deushi M, Mizuta R, Yabu S, Obata A, Nakano H, Koshiro T, Ose T, Kitoh A (2012) A New Global Climate Model of the Meteorological Research Institute: MRI-CGCM3;Model Description and Basic Performance. Journal of the Meteorological Society of Japan 90A (0):23-64. doi:10.2151/jmsj.2012-A02

Table 1: Details of CMIP5 models used in this study

Model	Horizontal grids (latxlon)	Reference
BCC-CSM1-1	64x128	Wu (2012)
CanESM2	64x128	Chylek et al. (2011)
CCSM4	192x288	Gent et al. (2011)
CESM1-BGC	192x288	Riley et al. (2011)
CESM1-WACCM	96x144	Richter et al. (2008)
GFDL-CM3	90x144	Griffies et al. (2011)
GFDL-ESM2G	90x144	Dunne et al. (2012)
GFDL-ESM2M	90x144	Dunne et al. (2012)
MIROC5	128x256	Watanabe et al. (2010)
MRI-CGCM3	160x320	Yukimoto et al. (2012)
NorESM1-M	96x144	Bentsen et al. (2012)
NorESM1-ME	96x144	Tjiputra et al. (2012)

Table 2: Decadal change of global averaged surface temperature (δTS) for 1996–2005 average minus 1901–1910 average and associated scaled changes in column integrated water vapor (δw), Precipitation (δP), and Convective mass flux (ΔM_c).

Clausius-Claperyon scaling for $\delta w/\delta TS$ is ~7% K^{-1} assuming constant relative humidity.

Experiment/Variable	δTS (K)	$\delta w/\delta TS$ (% K^{-1})	$\delta P/\delta TS$ (% K^{-1})	$\Delta M_c/\delta TS$ (% K^{-1})
CMIP	0.90	7.4	1.2	-3.1
CTRL	0.91	7.0	1.6	-2.4
ENSO-rel	0.52	7.3	0.4	-4.7
ENSO-unrel	0.64	5.5	0.2	-2.4

Table 3: Spatial correlations over tropical Oceanic region between trend maps of SLP, ω_{500}, M_c, and TS simulated by CAM4 CTRL (Green boxes), CMIP5 (blue boxes), and those between trend maps of respective variables simulated by CAM4 CTRL and CMIP5 (yellow boxes).

Variable	SLP	ω_{500}	M_c	TS
SLP	0.36	0.41	-0.38	-0.73
ω_{500}	0.46	-0.01	-0.91	-0.46
Mc	-0.34	-0.85	0.07	0.49
TS	-0.40	-0.34	0.52	0.03

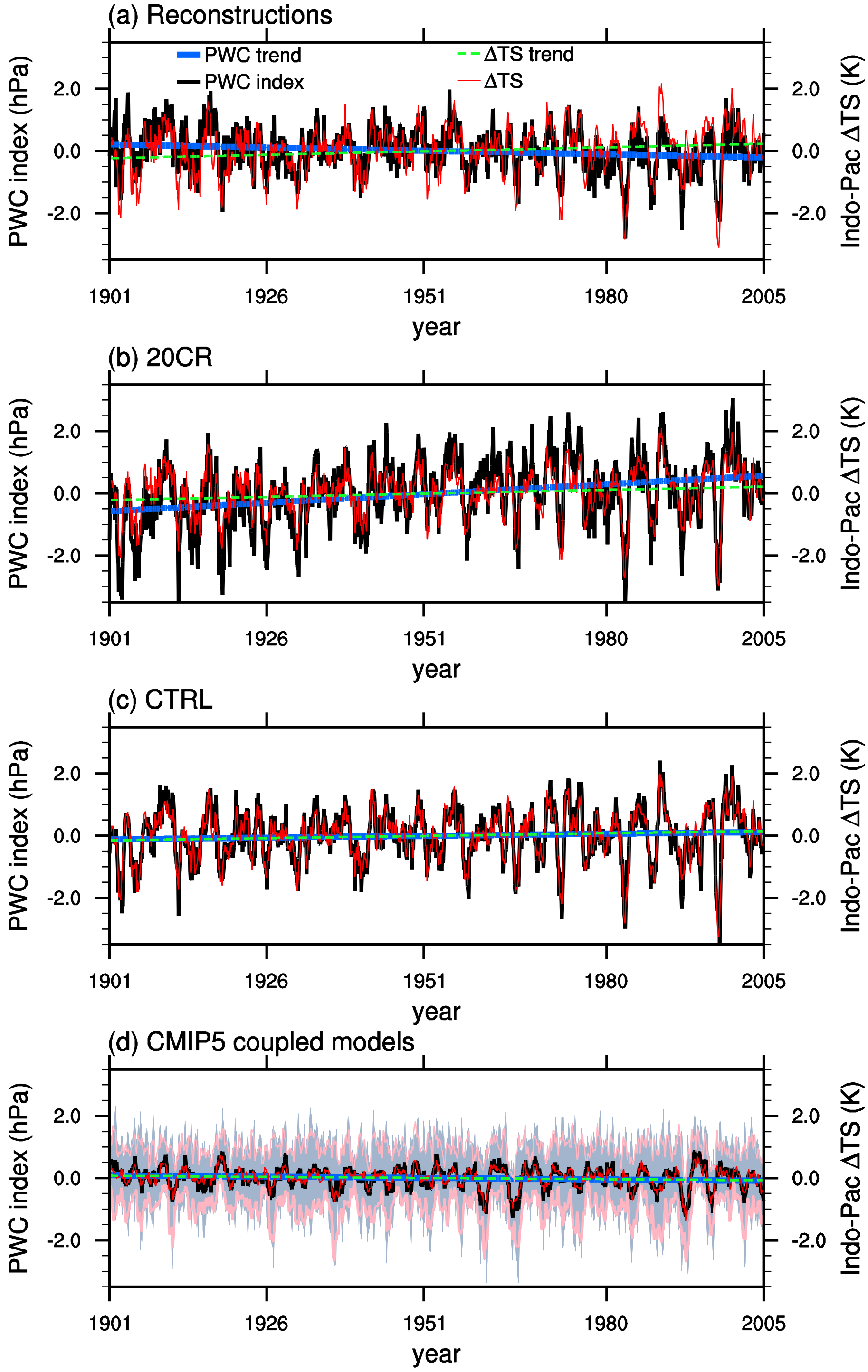

Figure 1: Pacific Walker Circulation (PWC, black curve) index and Pacific East West Temperature difference (ΔTS, red curve) of regions in Fig. 6a from (a) Reconstructions, (b) 20CR, (c) CAM4 CTRL ensemble , and (d) CMIP5 models (Table 1). Blue (green dashed) line shows the least-squares linear trend fit to the PWC (ΔTS).

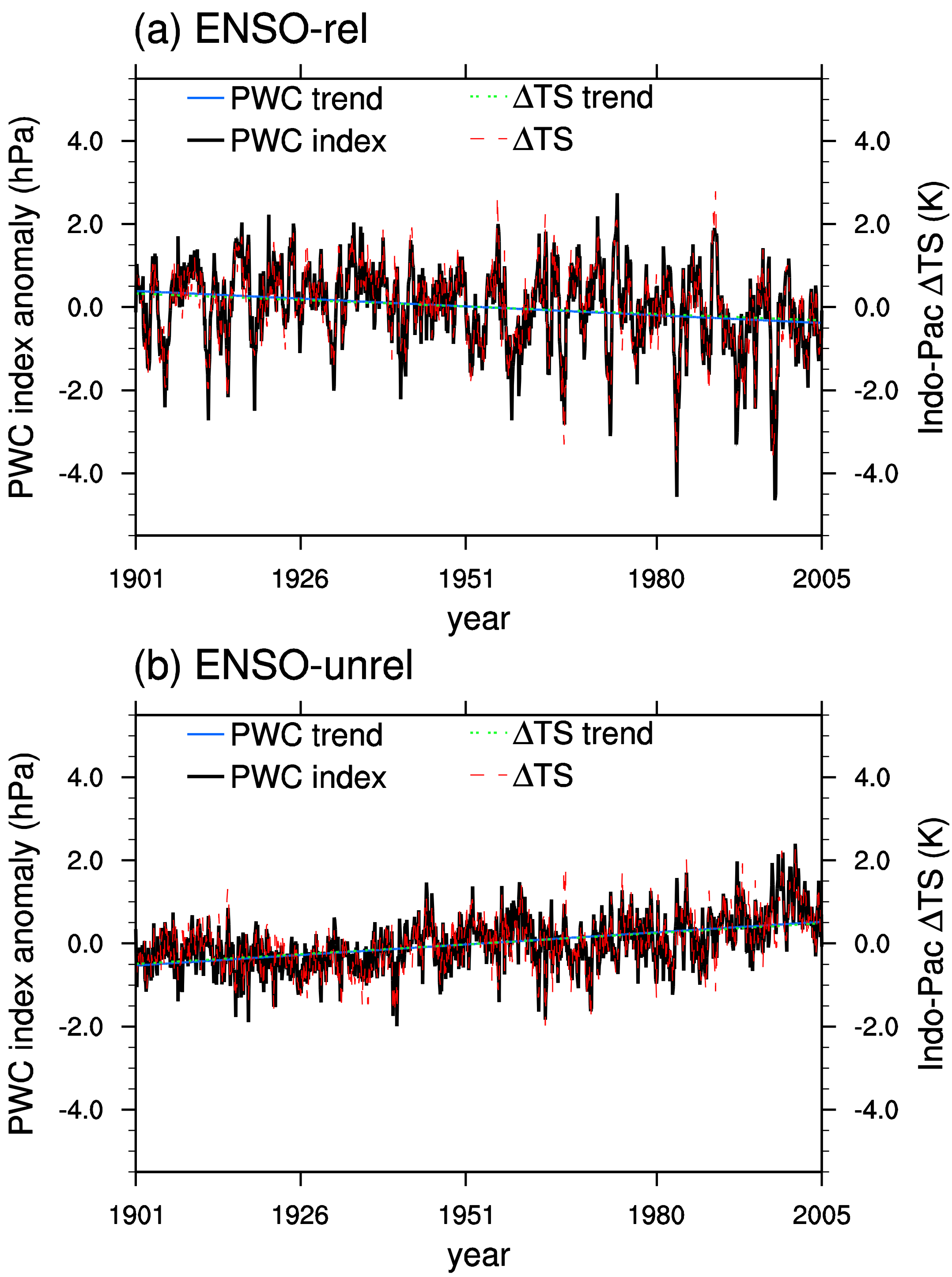

Figure 2: Ensemble mean PWC index (black curve) and ΔTS (red dashed curve) from CAM4 simulations of (a) ENSO-related SST and (b) ENSO-unrelated SST. Blue (green dashed) line shows the least-squares linear trend fit to the PWC (ΔTS).

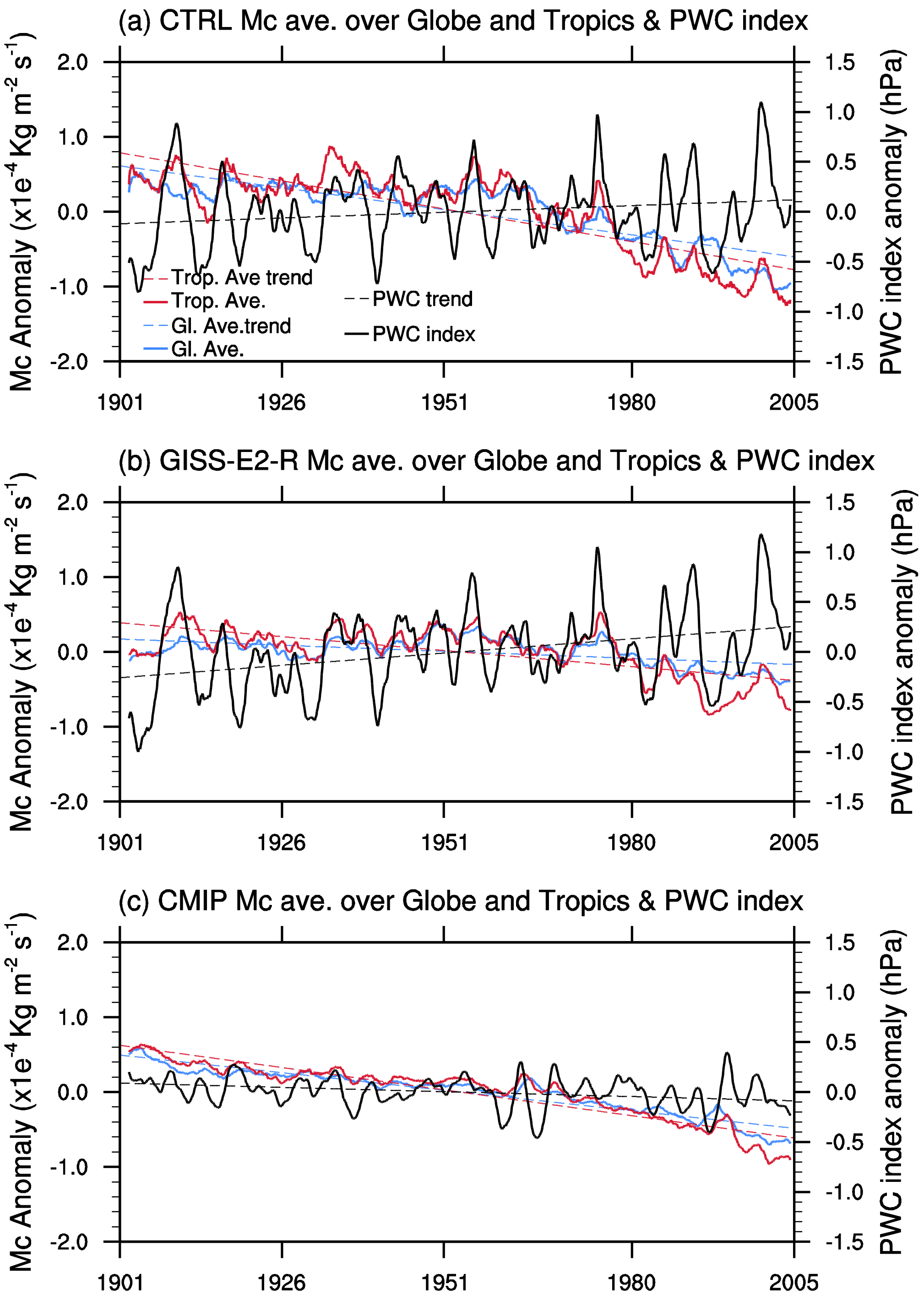

Figure 3: PWC index (black curve) and Convective mass flux anomaly M_c averaged over the globe (blue curve) and the tropics (red curve) from (a) CTRL and (b) GISS-E2-R, and (c) CMIP5 simulations. Black dashed line shows the least-squares linear trend fit to the PWC. Red (blue) dashed line shows the trend fit to the tropical (global) average M_c.

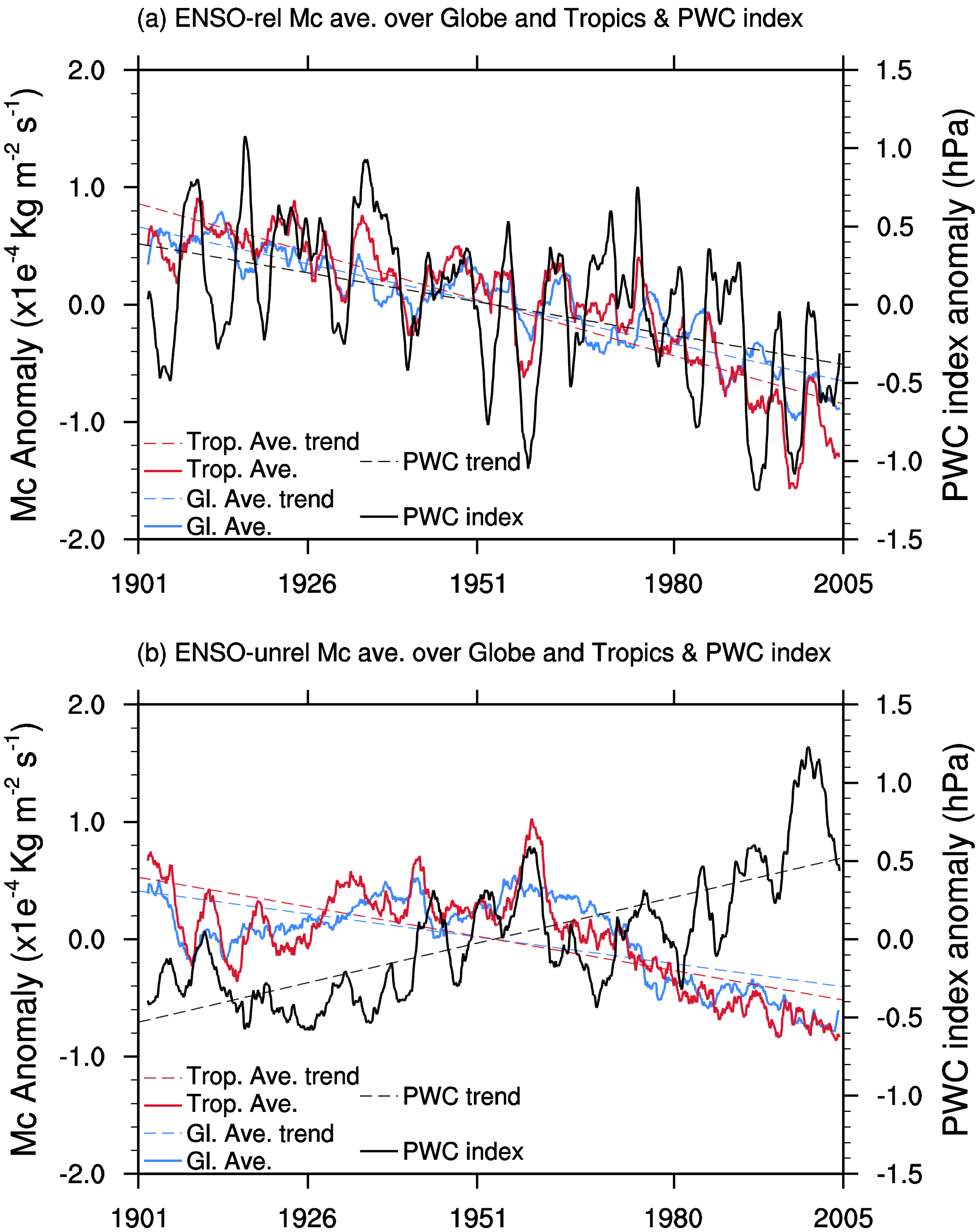

Figure 4: Same as Fig. 3, except for CAM4 simulations with ENSO-related and ENSO-unrelated SSTs

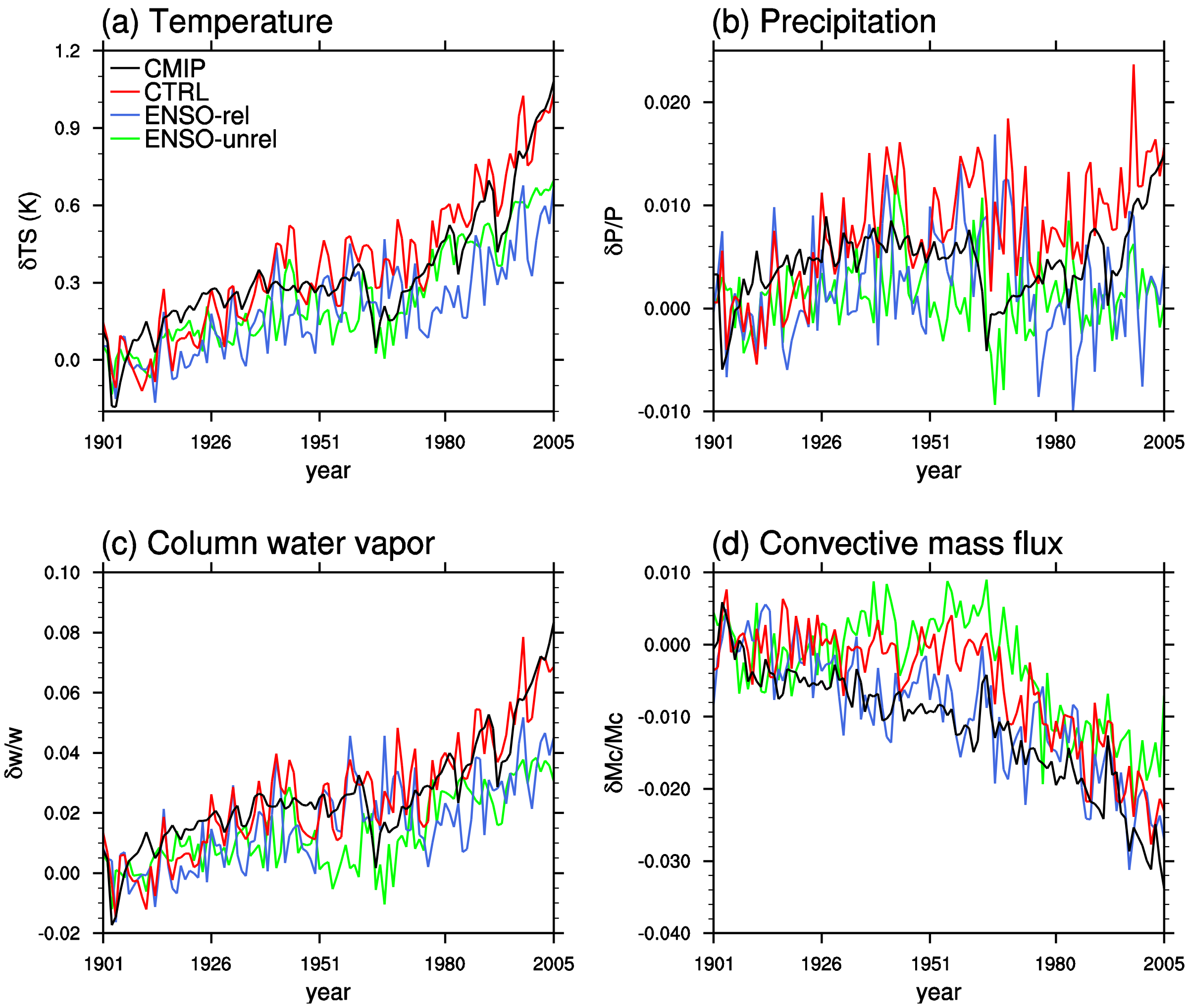

Figure 5: Time series of global mean changes in (a) temperature (K), (b) precipitation, (c) column integrated water vapor, and (d) convective mass flux. All quantities except temperature are expressed as fractional change relative to 1901 – 1910 mean. All quantities are annual means and are computed by first global averaging, and then differencing with the average computed over 1901 – 1910. Curves show results from the ensemble means of (black) CMIP5; (red) CAM4 CTRL; (blue) CAM4 forced with ENSO-related SSTs; (green) CAM4 forced with ENSO-unrelated SSTs.

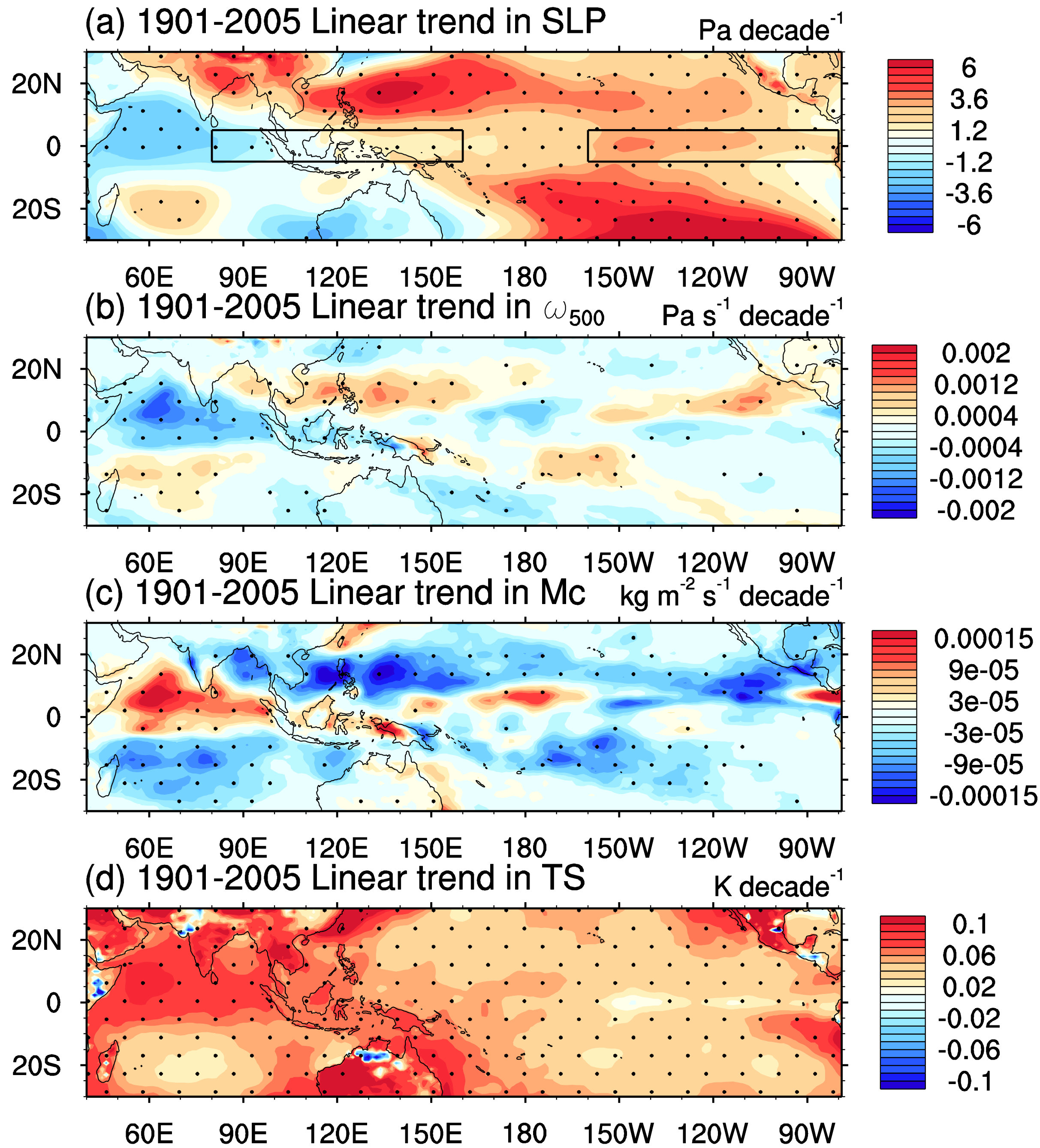

Figure 6: Spatial patterns of 1901-2005 trend in (a) SLP, (b) vertical velocity at 500 hPa, (c) convective mass flux, and (d) surface temperature from CTRL simulations. Stippling show trends that are statistically significant at 5% level, as revealed by a t-test. The boxes in (a) show the regions, over which SLP and TS are averaged for PWC index and ΔTS calculations. Negative values in 5b indicates upward motion.

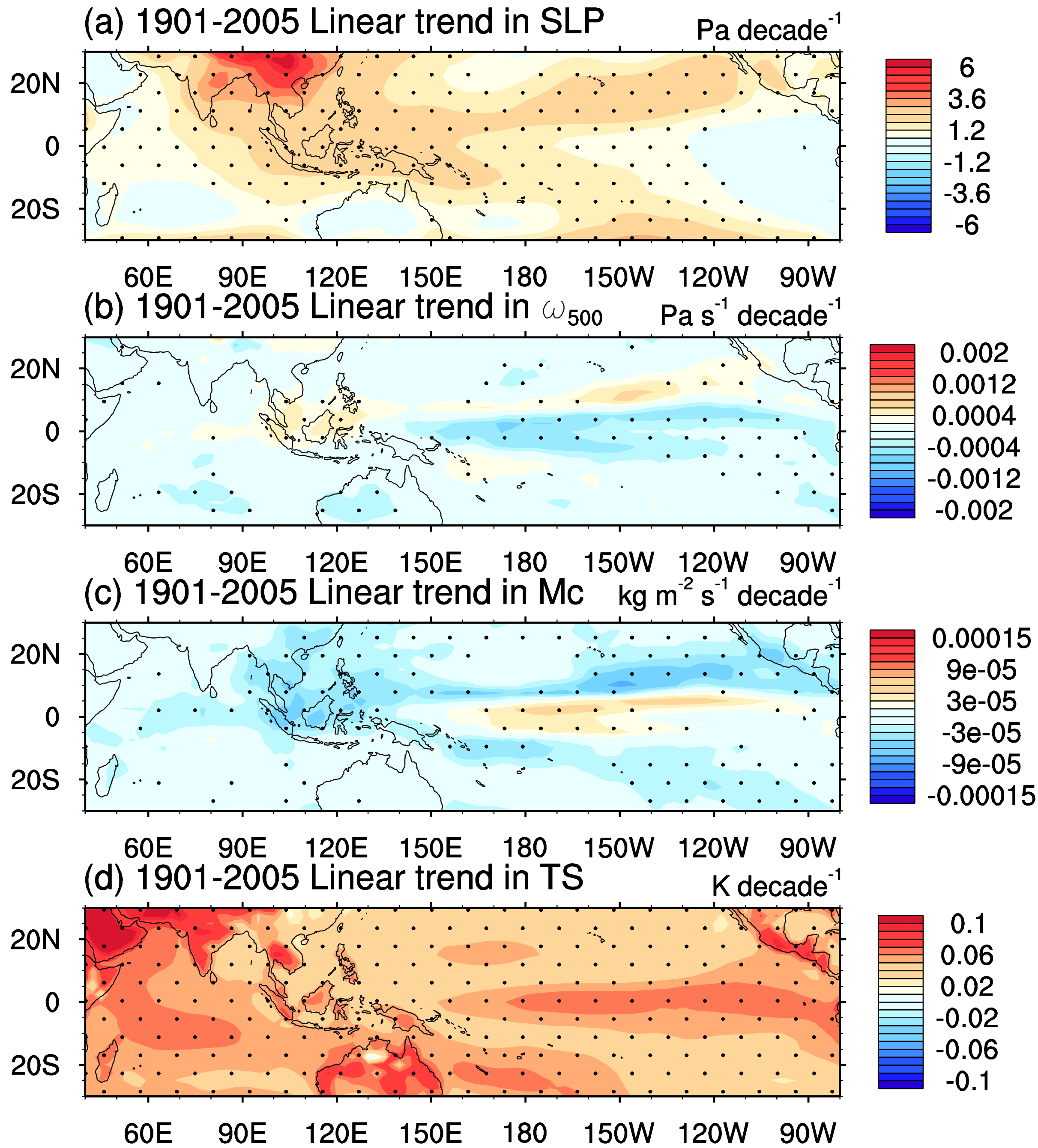

Figure 7: Same as Fig. 6, except for CMIP5 simulations

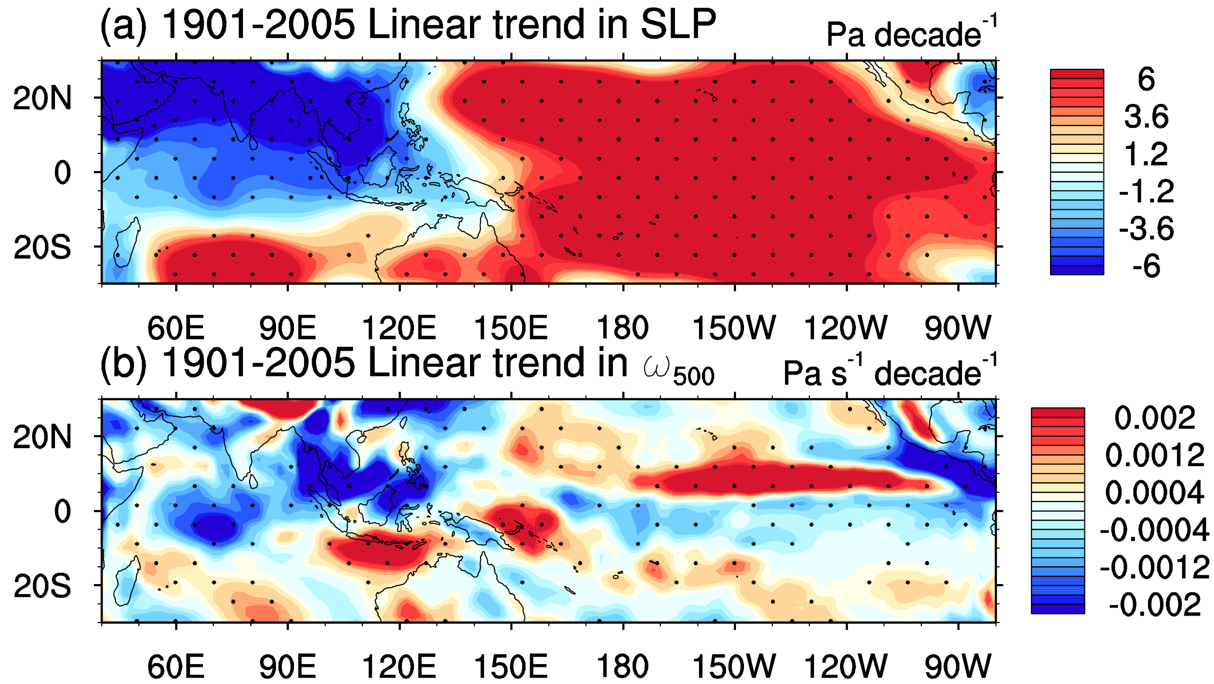

Figure 8: Spatial patterns of 1901-2005 trend in (a) SLP, (b) vertical velocity at 500 hPa calculated from 20CR. Stippling show trends that are statistically significant at 5% level, as revealed by a t-test.

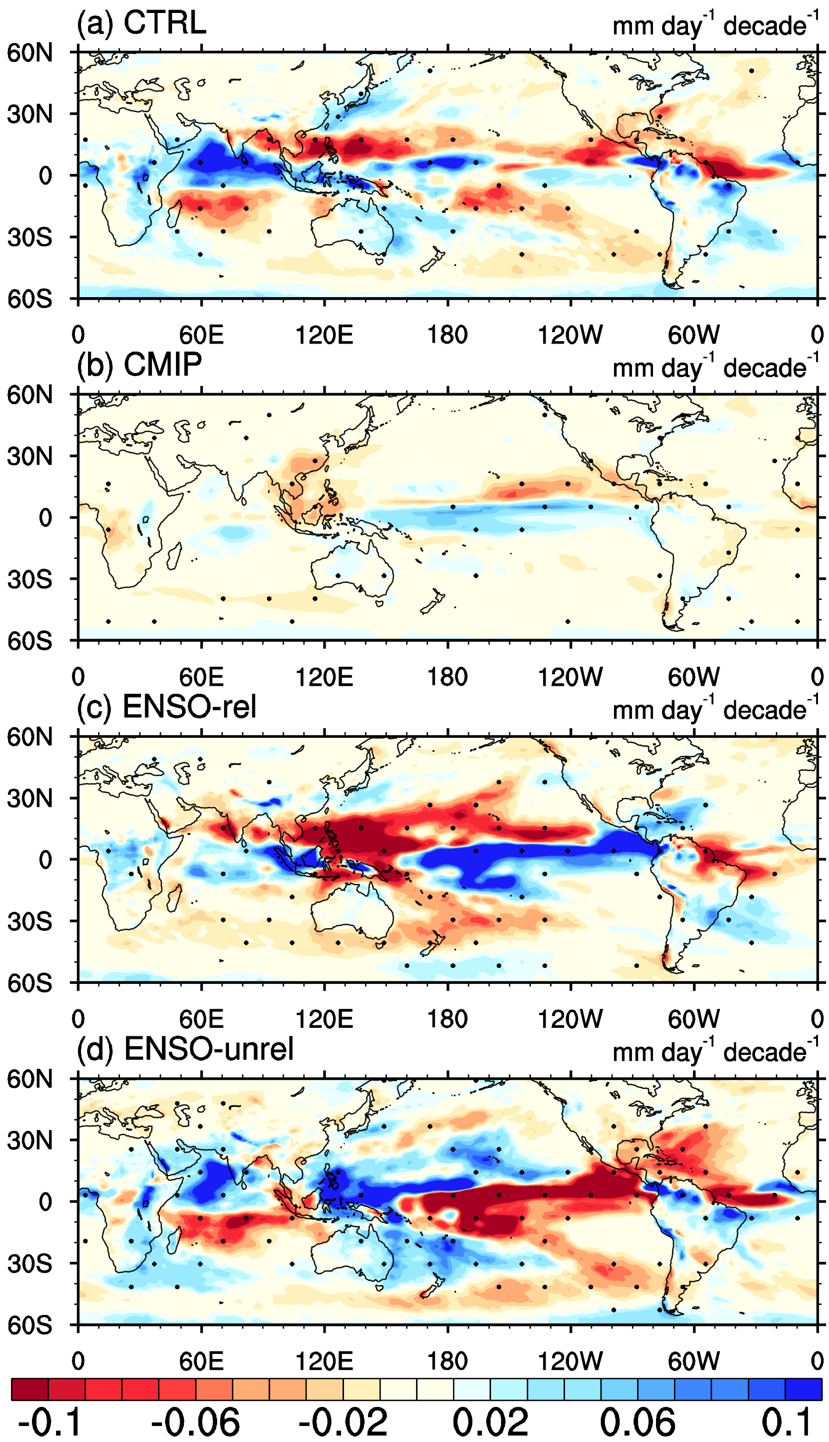

Figure 9: Spatial Patterns of trends in 1901-2005 precipitation from (a) CTRL, (b) CMIP5, (c) ENSO-related, and (d) ENSO-unrelated simulations.